JCTC Journal of Chemical Theory and Computation

Solvatochromic Shifts on Absorption and Fluorescence Bands of *N,N*-Dimethylaniline

Ignacio Fdez. Galván,*,† M. Elena Martín,† Aurora Muñoz-Losa,‡ and Manuel A. Aguilar†

Química Física, Edif. José María Viguera Lobo, Universidad de Extremadura, Avda. de Elvas s/n, 06071 Badajoz, Spain, and Dipartimento di Chimica e Chimica Industriale, Università degli Studi di Pisa, Via Risorgimento 35, 56126 Pisa, Italy

Received October 15, 2008

Abstract: A theoretical study of the absorption and fluorescence UV/vis spectra of *N,N*-dimethylaniline in different solvents has been performed, using a method combining quantum mechanics, molecular mechanics, and the mean field approximation. The transitions between the three lowest-lying states have been calculated in vacuum as well as in cyclohexane, tetrahydrofuran, and water. The apparent anomalies experimentally found in water (a blue shift in the absorption bands with respect to the trend in other solvents, and an abnormally high red shift for the fluorescence band) are well reproduced and explained in view of the electronic structure of the solute and the solvent distribution around it. Additional calculations were done with a mixture of cyclohexane and tetrahydrofuran as solvent, which displays a nonlinear solvatochromic shift. Results, although not conclusive, are consistent with experiment and provide a possible explanation for the nonlinear behavior in the solvent mixture.

1. Introduction

The nature and relative energies of the electronic states of a molecule determine its photophysical and photochemical properties. The environment in which a molecule is immersed can alter these states, which in turn modifies the properties, giving rise, for instance, to solvatochromic shifts in absorption and emission UV/vis spectra.[1] The experimental study of solvent effects on UV/vis spectra provides an important insight on the electronic properties of molecules, while their theoretical study represents an important challenge, since it requires both an accurate description of the internal structure of the solute and an appropriate modeling of the solvent structure and the solute−solvent interaction. The development of high-quality quantum methods capable of describing excited states (CASPT2, TD-DFT, etc.), together with convenient solvent models (PCM, RISM, MD, etc.), has allowed theoretical calculations of solvent effects to reach a high accuracy.

In our group, we have developed a method, called ASEP/MD (Averaged Solvent Electrostatic Potential from Molecular Dynamics) for including the solvent influence on quantum calculations.[2−4] This method has been successfully applied to the study of diverse properties and processes,[5−10] including UV/vis spectra.[11−14] In this paper, we carry out a study of solvent effects on the absorption and emission spectra of *N,N*-dimethylaniline (DMA), Figure 1. The solvatochromic shifts of the absorption and emission maxima of DMA in different solvents are in general proportional to the polarity function of the solvent ($f(\varepsilon) = 2(\varepsilon - 1)/(2\varepsilon + 1)$), but in water and other protic solvents this trend is broken. Additionally, in cyclohexane/tetrahydrofuran solvent mixtures, the solvatochromic shifts do not vary linearly with the molar fractions, as would be expected from the dielectric properties of the solvent.[1] We expect the ASEP/MD method to be able to correctly reproduce and explain these apparently anomalous behaviors, since it takes into account the explicit structure of the solvent and allows the use of accurate quantum methods. To attain these goals, it has been necessary to extend the method to work with solvent mixtures of arbitrary composition, which required only minimal changes in the previous software.

* E-mail: jellby@unex.es.
† Universidad de Extremadura.
‡ Università degli Studi di Pisa.

10.1021/ct800434j CCC: $40.75
Published on Web 01/15/2009

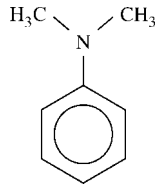

Figure 1. *N,N*-Dimethylaniline (DMA).

In section 2 we present a description of the methods and models used in this work, along with computational details. Section 3 contains the obtained results and discussion, divided into subsections gas phase, pure solvents, and solvent mixture. Finally, our conclusions are presented in section 4.

2. Methods and Details

Solvent effects on the DMA UV/vis spectra were calculated with ASEP/MD method. This is a sequential quantum mechanics/molecular mechanics (QM/MM) method implementing the mean field approximation. It combines, alternately, a high-level quantum mechanics (QM) description of the solute with a molecular mechanics (MM) description of the solvent. One of its main features is the fact that the solvent effect is introduced into the solute's wave function as an average perturbation. Details of the method have been described in previous papers,[2−4] so here we will only present a brief outline.

As mentioned above, ASEP/MD is a method combining QM and MM techniques, with the particularity that full QM and MD (molecular dynamics) calculations are alternated and not simultaneous. During the MD simulations, the intramolecular geometry and charge distribution of all molecules is considered as fixed. From the resulting data, the average electrostatic potential generated by the solvent on the solute (ASEP) is obtained. This potential is introduced as a perturbation into the solute's quantum mechanical Hamiltonian, and by solving the associated Schrödinger equation, one gets a new charge distribution for the solute, which is used in the next MD simulation. This iterative process is repeated until the electron distribution of the solute and the solvent structure around it are mutually equilibrated.

The ASEP/MD framework can also be used to optimize the geometry of the solute molecule.[5] At each step of the ASEP/MD procedure, the gradient and Hessian on the system's free-energy surface (including the Van der Waals contribution) can be obtained, and so they can be used to search for stationary points on this surface by some optimization method. After each MD simulation, the solute geometry is optimized within the fixed "average" solvent structure by using the free-energy derivatives. In the next MD simulation, the new solute geometry and charge distribution are used. This approach allows the optimization of the solute geometry simultaneously to the solvent structure.

For calculating transition energies, the iterative process is performed on the initial state of the transition (the ground-state for absorption, the excited-state for emission), i.e., the atomic charges for the MD and the energy derivatives for the geometry optimization of the solute are calculated with the initial state wave function. Then, with a frozen solvent model, the transition energies between the different states are obtained. It is also possible to calculate transition energies with a polarizable solvent model; in this case, once the solute and solvent structure have been optimized for the initial state of the solute, each state energy and wave function is calculated with the same solvent structure, but where the solvent molecules' charges are replaced by gas-phase charges plus a molecular polarizability.[11,13] In this work we used a nonpolarizable solvent model in all cases, as test calculations with polarizable solvent did not show an important enough influence to compensate the increased computational effort required.

With the transition energies calculated in solution and in gas phase, the solvent shift δ can be obtained as the difference:

$$\begin{aligned}\delta &= \Delta E - \Delta E^0 \\ &= (\langle \Psi_f|\hat{H}_{QM} + \hat{V}|\Psi_f\rangle - \langle \Psi_i|\hat{H}_{QM} + V|\Psi_i\rangle) - \\ &\quad (\langle \Psi^0_f|\hat{H}^0_{QM}|\Psi^0_f\rangle - \langle \Psi^0_i|\hat{H}^0_{QM}|\Psi^0_i\rangle) \\ &= (\langle \Psi_f|\hat{H}_{QM} + \hat{V}|\Psi_f\rangle - \langle \Psi^0_f|\hat{H}^0_{QM}|\Psi^0_f\rangle) - \\ &\quad (\langle \Psi_i|\hat{H}_{QM} + \hat{V}|\Psi_i\rangle - \langle \Psi^0_i|\hat{H}^0_{QM}|\Psi^0_i\rangle) \end{aligned} \quad (1)$$

where the subindices i and f denote the initial and final state, $\hat{H}_{QM}$ is the QM Hamiltonian of the solute at the in-solution geometry, without the solute−solvent interaction, $\hat{V}$, and $\hat{H}^0_{QM}$ is the QM Hamiltonian at the gas-phase geometry; Ψ and Ψ^0 are, respectively, the wave functions optimized in solution and in gas phase. This solvent shift can be partitioned in different contributions, namely a geometry contribution δ_{geo}, an electronic distortion contribution δ_{dist}, and an electrostatic solute−solvent contribution δ_{elec}. If we introduce Ψ' as the wave function optimized for the $\hat{H}_{QM}$ Hamiltonian:

$$\begin{aligned}\delta &= \delta_{geo} + \delta_{dist} + \delta_{elec} \\ \delta_{geo} &= (\langle \Psi'_f|\hat{H}_{QM}|\Psi'_f\rangle - \langle \Psi^0_f|\hat{H}^0_{QM}|\Psi^0_f\rangle) - \\ &\quad (\langle \Psi'_i|\hat{H}_{QM}|\Psi'_i\rangle - \langle \Psi^0_i|\hat{H}^0_{QM}|\Psi^0_i\rangle) \\ \delta_{dist} &= (\langle \Psi_f|\hat{H}_{QM}|\Psi_f\rangle - \langle \Psi'_f|\hat{H}_{QM}|\Psi'_f\rangle) - \\ &\quad (\langle \Psi_i|\hat{H}_{QM}|\Psi_i\rangle - \langle \Psi'_i|\hat{H}_{QM}|\Psi'_i\rangle) \\ \delta_{elec} &= \langle \Psi_f|\hat{V}|\Psi_f\rangle - \langle \Psi_i|\hat{V}|\Psi_i\rangle \end{aligned} \quad (2)$$

Thus, δ_{geo} is the solvent shift due to the change in geometry between gas phase and solution, δ_{elec} corresponds to the difference in solute−solvent interaction energy between the initial and final states, and δ_{dist} corresponds to the difference in the wave function distortion energy. For convenience, fluorescence energies are reported as positive values, although they would be negative when eq 1 is applied. Similarly the δ values for fluorescence are given as positive numbers for blue shifts and negative for red shifts. Note that the Van der Waals component of the interaction energy is not included in the above expressions, since we adopt the approximation of considering it constant for all electronic states of the solute, and therefore it vanishes when vertical transition energies are considered.

The quantum calculations of the solute molecule were done with the complete active space self-consistent field (CAS-SCF) method,[15] using the 6−311G** basis set. Gas-phase calculations were also done with 6−31G**, cc-pVDZ, and

6−311++G** basis sets. The active orbitals were the six π and π^* orbitals of the phenyl ring and the nonbonded orbital of the nitrogen, and eight electrons were included in these orbitals, for an (8,7) total active space. Geometry optimizations in gas phase and in solution were performed on pure roots (the ground state, S_0, or the first excited singlet state, S_1), but transition energies were always calculated with a state-average (SA) calculation of the first three singlet states, S_0, S_1, and S_2. To obtain accurate transition energies, it is known that the inclusion of dynamic correlation in the quantum calculations is necessary, which we did with the complete active space second-order perturbation (CASPT2) method,[16,17] using the SA-CASSCF(8,7) wave functions as reference. A new IP−EA shifted zeroth-order Hamiltonian has been recently proposed for CASPT2 calculations,[18] which is supposed to reduce systematic overstabilization errors in open-shell systems (as in the excited states). We did all CASPT2 with the proposed IP−EA shift of 0.25 E_h (CASPT2 (0.25)) as well as with no IP−EA shift (CASPT2(0.00)). To minimize the appearance of intruder states, an additional imaginary shift of 0.1i E_h was used. No symmetry was assumed in any case.

The MD simulations were carried out with rigid molecules; cyclohexane, tetrahydrofuran, and water were used as solvents. Lennard-Jones parameters and solvent atomic charges were taken from the OPLS-AA force field,[19] and solute atomic charges were calculated from the quantum calculations with the CHELPG method.[20] The geometry of cyclohexane and tetrahydrofuran were optimized with B3LYP/6−311G**; for water, the TIP3P model was employed. An amount of 216 solvent molecules and the solute were included in a cubic simulation box (800 water molecules for aqueous solution) at the experimental density of the solvent.[21] Periodic boundary conditions were applied, and spherical cutoffs were used to truncate the interatomic interactions at 12 Å; long-range interactions were calculated using the Ewald sum technique. The temperature was fixed at 298 K by using the Nosé−Hoover thermostat. A time step of 0.5 fs was used during the simulations, and each one was run for 100 ps after 25 ps equilibriation.

At each step of the ASEP/MD procedure, 500 configurations evenly distributed from the MD run were used to calculate the ASEP and a radius of 15 a_0 (12 a_0 for water) was used for including explicit solvent charges. Each ASEP/MD run was continued until the energies and solute geometry and charges are stabilized for at least five iterations; results are reported as the average of these last five iterations.

For in-solution calculations, the ASEP/MD software[3] was used, with the needed modifications to allow the use of more than one solvent species. During the ASEP/MD runs, quantum calculations (CASSCF optimizations) were performed with the Gaussian 98 package.[22] The final SA-CASSCF and CASPT2 calculations were done with Molcas 6.4.[23] All MD simulations were performed using Moldy.[24]

3. Results and Discussion

3.1. Gas Phase. The geometry of DMA was optimized in gas phase, at CASSCF/6−311G** level, for both the ground state (S_0) and the first excited state (S_1). In agreement with experimental results,[25] the obtained S_0 geometry is pyramidal in the N, with a CH_3-N-CH_3 angle of 114.7° (experimental: 114°) and a wagging angle (the angle between the phenyl ring plane and the CH_3-N-CH_3 plane) of 28.4° (experimental: 27.0°), the N atom being slightly (0.059 Å) out of the phenyl ring plane (see Figure 2). These geometrical parameters are mantained (to within 0.4°, 0.6°, and 0.004 Å, respectively) when the optimization is carried out with the 6−31G**, cc-pVDZ, and 6−311++G** basis sets.

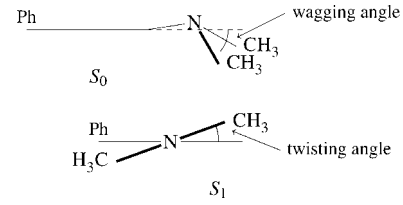

Figure 2. Scheme showing the wagging and twisting angles in the ground and excited states of DMA.

Table 1. Absorption Energies Calculated in Gas Phase, in eV (oscillator strength in parentheses)

	SA-CASSCF		CASPT2(0.25)		CASPT2(0.00)	
	$S_0\rightarrow S_1$	$S_0\rightarrow S_2$	$S_0\rightarrow S_1$	$S_0\rightarrow S_2$	$S_0\rightarrow S_1$	$S_0\rightarrow S_2$
6−31G**	4.82	7.11	4.77 (0.010)	5.73 (0.267)	4.41 (0.010)	5.27 (0.246)
cc-pVDZ	4.79	6.99	4.71 (0.011)	5.57 (0.268)	4.33 (0.010)	5.09 (0.245)
6−311G**	4.80	6.99	4.69 (0.010)	5.54 (0.269)	4.30 (0.009)	5.06 (0.245)
6−311++G**	4.78	6.85	4.65 (0.008)	5.32 (0.277)	4.30 (0.007)	4.87 (0.253)
experimental[26]	4.30 (0.044)	5.16 (0.256)				

The transition energies to the S_1 and S_2 states, at the CASSCF optimized S_0 geometry were calculated with a state-average CASSCF method (including the first three roots), and with perturbation theory using both CASPT2(0.25) and CASPT2(0.00). The results are displayed in Table 1; it is clear that both absorption energies are overestimated at SA-CASSCF level, but the CASPT2 method yields results in good agreement with the experiment. As expected, the transition energies with CASPT2(0.25) are larger than with CASPT2(0.00), the latter results being closer to the experimental values. However, given that CASPT2(0.25) results approach the experimental reference when the basis set quality is improved, the good performance of CASPT2(0.00) in this case is probably due to error cancelation, especially for the $S_0\rightarrow S_2$ transition.

The oscillator strengths for the two transitions $S_0\rightarrow S_1$ and $S_0\rightarrow S_2$ are also in very good agreement with the experimental estimations and are much less dependent on the basis set and method. They indicate that the transition to S_1 has a weak intensity while that to S_2 is much more favored. According to the assignment of Kimura et al.,[26] the main contribution to the S_1 state would correspond to a local excitation in the phenyl ring, while S_2 stems from an intramolecular charge transfer between the $N(CH_3)_2$ electron donor and the phenyl acceptor. This assignment is confirmed by the calculated dipole moments of the three states, being at CASPT2(0.25)/6−311G** level, 1.33 D for S_0, 1.66 D for S_1, and 5.98 D

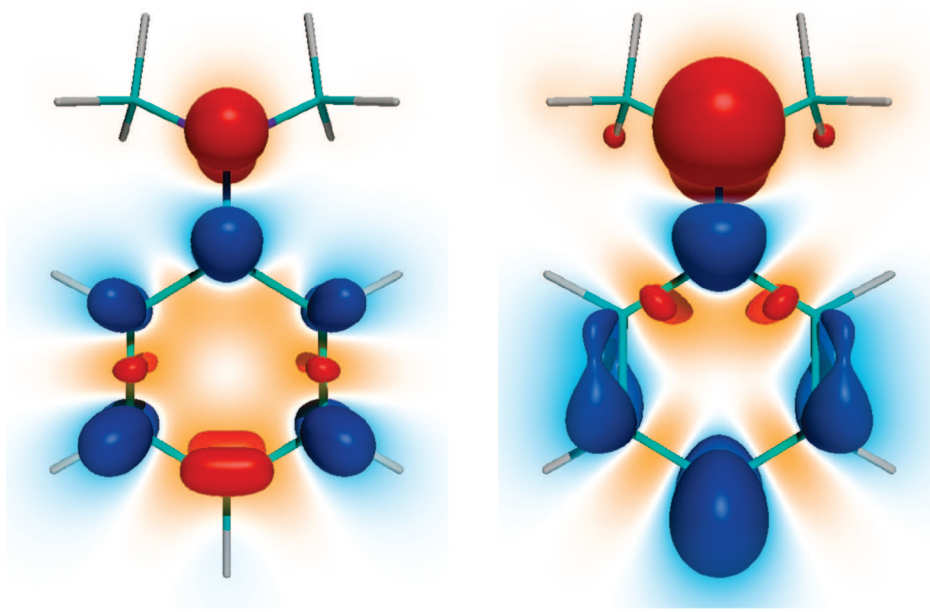

Figure 3. Electron density change in the $S_0 \rightarrow S_1$ transition (a) and in the $S_0 \rightarrow S_2$ transition (b). Isosurfaces for a change of $\pm$ 0.0032, red for a decrease in density, blue for an increase. Densities calculated at SA-CASSCF/6−311G** level.

for S_2, in all cases directed from the phenyl ring to the nitrogen and toward the side of the ring plane where the methyl groups lie. Electron density differences between the ground state and S_1 and S_2 are displayed in Figure 3; they clearly show the important charge-transfer nature of the S_2 state. There is also some transfer component in S_1, but it is not so drastic. The Mulliken populations confirm a flux of 0.28 electrons from $N(CH_3)_2$ to the phenyl for the $S_0 \rightarrow S_2$ transition and only 0.05 electrons for $S_0 \rightarrow S_1$.

The CASSCF/6−311G** optimization of the S_1 state yields a planar structure of the N atom, but the CH_3-N-CH_3 plane is now twisted 19.5° with respect to the phenyl ring (Figure 2) and the CH_3-N-CH_3 angle is 115.9°. Again the other basis sets give similar results. This planar and twisted structure in the excited state agrees with the interpretation of the experimental spectrum given by Saigusa et al.,[27] who conclude a torsion angle of 26°. These authors suggest a pyramidal N atom (with a wagging angle of 13°) but with an inversion barrier so low that it would lie below zero-point energy, and thus the S_1 state of DMA could be considered planar in the N atom.

Table 2 collects the calculated band origins (0−0 transition) and fluorescence energies ($S_1 \rightarrow S_0$) obtained with the different methods and basis sets, with the optimized S_0 and S_1 geometries. Similarly to the absorption energies, SA-CASSCF overestimates the transition energies and the difference between CASPT2(0.25) and CASPT2(0.00) is quite constant, around 0.3−0.4 eV. Again, with increasing basis set quality CASPT2(0.25), results seem to improve.

It was also possible to optimize an untwisted pyramidal geometry for S_1, similar to the S_0 structure, with a wagging angle of 19.5°. At CASPT2(0.00)//CASSCF/6−311G** level, this wagged minimum is 0.03 eV higher in energy than the planar twisted one, its $S_1 \rightarrow S_0$ transition energy is 0.12 eV larger, and its dipole moment is ∼0.2 D lower. The lower energy of the twisted minimum and its fluorescence energy more in agreement with the experimental results available make this structure the most likely for the excited-state of DMA, in line with the conclusions of Saigusa et al.[27] Moreover, the higher dipole moment would additionally favor the twisted minimum in solution, as it would be better stabilized by the solvent. The wagged minimum may be an artifact of the CASSCF optimization and it might not appear if the optimization were performed at CASPT2 level. In the rest of this paper we always consider the planar twisted structure for the optimized S_1 state.

Table 2. Band Origins and Fluorescence Energies Calculated in Gas Phase, in eV (oscillator strength in parentheses)

	SA-CASSCF		CASPT2(0.25)		CASPT2(0.00)	
	0−0	$S_1 \rightarrow S_0$	0−0	$S_1 \rightarrow S_0$	0−0	$S_1 \rightarrow S_0$
6−31G**	4.61	4.34	4.52	4.26 (0.015)	4.15	3.90 (0.014)
cc-pVDZ	4.59	4.32	4.40	4.20 (0.018)	4.01	3.82 (0.016)
6−311G**	4.60	4.32	4.41	4.17 (0.018)	4.01	3.79 (0.016)
6−311++G**	4.57	4.31	4.37	4.14 (0.016)	4.00	3.79 (0.015)
experimental	4.08[a]	3.69[b] ∼3.87[c]				

[a] Reference 27. [b] Reference 28 in *n*-hexane. [c] Reference 29 in *n*-hexane (estimated from graph).

3.2. Pure Solvents. The DMA geometry was also optimized in solution, using cyclohexane (CH), tetrahydrofuran (THF), and water as solvents. As in the gas-phase study, the $S_0 \rightarrow S_1$ and $S_0 \rightarrow S_2$ absorption energies were calculated with the optimized S_0 structure, while the $S_1 \rightarrow S_0$ fluorescence energy was calculated only with the planar twisted S_1 structure.

Table 3. Characteristic Angles (in degrees) and Dipole Moments (at CASPT2(0.00)/6-311G** level, in D) for Optimized Geometries of DMA[a]

	S_0 geometry				S_1 geometry		
	wag	$\mu(S_0)$	$\mu(S_1)$	$\mu(S_2)$	twist.	$\mu(S_0)$	$\mu(S_1)$
gas	28.4	1.34	1.68	5.98	19.5	1.62	2.19
cyclohexane	28.7	1.34	1.67	5.95	19.0	1.64	2.21
CH/THF (0.5)	28.5	1.41	1.77	6.05	18.5	1.91	2.53
tetrahydrofuran	28.5	1.56	1.93	6.25	18.1	2.10	2.78
water	34.0	1.56	1.77	5.83	15.8	3.23	4.56

[a] For the S_0 geometry, the wagging angle is given; for the S_1 geometry, the twisting angle is given.

The optimized wagging and twisting angles, as well as the dipole moments of the different states in the solvents considered are given in Table 3. As with the gas-phase calculations, the geometry was optimized with the CASSCF method, energies and dipoles were then calculated at SA-CASSCF and CASPT2 level, and only the 6−311G** basis set was used. The table shows a trend in the gas phase, cyclohexane, and tetrahydrofuran results: CH values are very similar to gas phase, while THF, with stronger polarity, originates an increase in the dipole moments, more important in the S_1 optimization. The changes in the wagging and twisting angles are negligible. In water, however, the behavior is different. In the S_0 geometry the pyramidalization of the N is enhanced and the dipole moments do not increase from the THF values; on the contrary, they decrease for the excited states. In the S_1 geometry, the changes in the twisting angle and in the dipole moments go in the same direction as with the other solvents, but they are much more important. These results already indicate a certain anomaly for DMA when dissolved in water, as will be seen in the transition energies.

Different estimations for the dipole moment difference between the ground and excited states, based on experimental solvatochromic and thermochromic shifts, have proposed values of 3.5 D,[30] 3.27 D,[31] or 1.89 D−1.99 D.[32] Our results cast doubt on the validity of these estimations, as we obtain a dipole moment difference between 0.9 and 1.2 D (S_0 and S_1 at their respective minima), and much lower if we consider the dipole moment increase upon excitation (S_0 and S_1 at the ground-state minimum). Only in water is the dipole moment difference 3 D, but the experimental data refer only to less polar solvents. In our opinon, the disagreement between our values and the experimental estimations shows the errors associated to the assumptions of the above-mentioned works, which basically rely on the Onsager solvation model.

The different transition energies calculated in solution are detailed in Table 4. As expected, the values obtained in cyclohexane are almost identical to the gas-phase results, with just a very slight (0.01 eV) blue shift in the absorption bands. This contrasts with the somewhat more sizable red shift (∼0.1 eV) found experimentally in all three transitions studied.[31,33] There are several possible sources for this error.

(1) The calculations did not consider the solvent electronic polarization in response to the electron transition in the solute. We did some test calculations with the polarizable version of ASEP/MD, in cyclohexane, and we obtained only a very small red shift (∼0.02 eV) with respect to the nonpolarizable calculations. This is therefore not enough to explain the discrepancy between the experimental and the calculated transition energies in solution.

Table 4. Transition Energies, in eV, Calculated in Solution at CASPT2(0.00)/6-311G** level (experimental values in parentheses)

	$S_0 \rightarrow S_1$	$S_0 \rightarrow S_2$	$S_1 \rightarrow S_0$
gas	4.30 (4.30)[a]	5.06 (5.16)[a]	3.79
cyclohexane	4.31 (4.22)[b]	5.07 (5.02)[b]	3.79 (∼3.72)[c]
CH/THF (0.5)	4.30	5.05	3.75
tetrahydrofuran	4.29	5.03	3.73
water	4.39 (4.28)[d]	5.15 (∼5.10)[e]	3.47 (3.40)[d]

[a] Reference 26. [b] Reference 31. [c] Reference 33 (estimated from graph). [d] Reference 34. [e] Reference 35 (estimated from graph).

(2) The neglect of the dispersion component of the transition energies. This component is known[36] to decrease transition energies in solution, since, in general, excited states are better stabilized by dispersion. There is, however, no accurate way to include the dispersion component in the calculations other than including a number of solvent molecules in the quantum system, which makes it difficult to estimate the contribution of this component. Nevertheless, the dispersion component depends mainly, in what regards the solvent, on the refractive index, and since this is quite constant in the studied solvents (1.33−1.43), we can expect the dispersion contribution to be similar in all cases. This would result in solvent differences and trends being well reproduced.

The transition energies obtained in tetrahydrofuran show a small red shift with respect to the cyclohexane values. The shift is larger for the $S_1 \rightarrow S_0$ transition (0.06 eV) and smaller for the $S_0 \rightarrow S_1$ transition (0.02 eV). This red shift is expected, considering the higher dipole moment of the excited states of DMA and the increased polarity of THF. The experimental data available[1] confirm the increased red shift both in absorption and fluorescence bands.

This trend, higher solvent polarity gives a larger red shift, is broken when the solvent is water (see Figure 4). In this case there are "anomalies" both in the absorption and emission energies, as happened with the geometry and dipole moments, commented above. In the absorption bands there is a blue shift of 0.08 eV when the cyclohexane and water solvents are compared, which would not be expected on the basis of the solvent polarity alone. In the fluorescence band, the red shift observed in water is much larger (0.32 eV) than what could be expected from polarity, too. These two anomalies are also found experimentally. The blue shift in absorption is also observed with other protic solvents such as alcohols, while the extraordinarily high red shift in fluorescence is only found in water.[1]

It is interesting to note that the error in the calculated values of the transition energies is very similar in cyclohexane and in water, despite being such disparate solvents. This fact points to the dispersion component as mainly responsible for the error in the computed transition energies in solution,

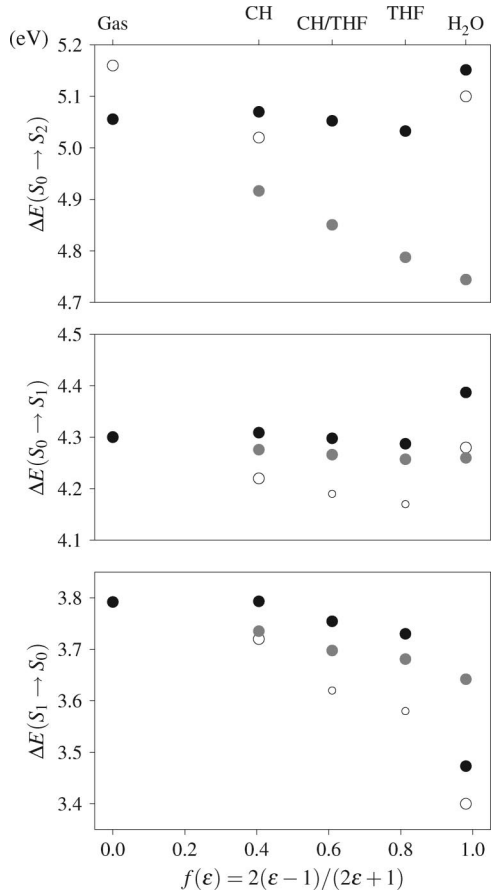

Figure 4. Transition energies for DMA in gas phase and different solvents, from Tables 4 and 5. Grey circles are PCM values, black circles are ASEP/MD or gas-phase values, and white circles are experimental values. The small white circles are obtained from Figure 12 in ref 1, considering the difference with respect to cyclohexane.

Table 5. Transition Energies, in eV, Calculated in Solution, with PCM, at CASPT2(0.00)/6-311G** Level

	$S_0 \rightarrow S_1$	$S_0 \rightarrow S_2$	$S_1 \rightarrow S_0$
cyclohexane	4.28	4.92	3.74
CH/THF (0.5)	4.27	4.85	3.70
tetrahydrofuran	4.26	4.79	3.68
water	4.26	4.74	3.64

since, as noted above, the magnitude of this component is expected to be quite similar in the different solvents. Thus, the trends in solvation are very well reproduced, as can be seen in Figure 4 if the differences with respect to cyclohexane are considered. Also, the error is similar for the absorption and emission energies, which translates in the calculated Stokes shifts being in excellent agreement with experimental values: 0.52 eV (exp. 0.50 eV) in cyclohexane, 0.92 eV (exp. 0.88 eV) in water. It is also worth mentioning that CASPT2(0.25) values for the transition energies (not given in Table 4) were in all cases 0.39 eV higher for the $S_0 \rightarrow S_1$ and $S_1 \rightarrow S_0$ transitions, and 0.48 eV higher for the $S_0 \rightarrow S_2$ absorption.

The observed anomalies are not explained by continuum models, such as the Polarizable Continuum Model (PCM).[37,38] For comparison, we carried out PCM calculations of the three studied transitions; the results are shown in Table 5. As before, the geometries were optimized at CASSCF(8,7)/6−311G** level, and the final energies were calculated with SA-CASSCF and CASPT2. To compare with the nonpolarizable ASEP/MD calculations, the fast polarization component in PCM was neglected, i.e., all solute states were calculated with the solvent charges in equilibrium with the initial state (S_0 for absorption, S_1 for fluorescence). The $S_0 \rightarrow S_1$ and $S_1 \rightarrow S_0$ transition energies are slightly smaller than with ASEP/MD, but the differences between cyclohexane and tetrahydrofuran are very similar. In the $S_0 \rightarrow S_2$ transition, the difference is larger and the calculated values are further from experiments. As expected, in all cases, the results with water follow the general trend and do not show the anomalies described above (see Figure 4). We also calculated the transition energies in vacuo with the PCM-optimized solute geometries, and we did not find significant differences, in any of the solvents, compared to the gas-phase transition energies. The increase in wagging angle in the ground-state in water is significantly smaller with PCM (2.5°) than with ASEP/MD (5.6°). For the excited state, the change in the twisting angle is stronger with PCM, but this is compensated for with a less out-of-plane position of the hydrogens in the ortho positions.

The behavior of the electron transitions in water must be therefore associated to specific interactions between the water molecules and the solute and not only to the bulk properties (polarity) of the solvent. The described anomalies are compatible with (a) a specific strong stabilization of the ground-state through O−H···N hydrogen bonds, which is lost when the excitation to S_1 or S_2 occurs, and (b) an increased stabilization of the S_1 state before fluorescence, probably through solvation of the phenyl ring, which is also lost when the relaxation to S_0 takes place.

In order to gain a deeper insight on the reasons for the behavior in water, we first performed gas-phase calculations with the geometries optimized in solution, which allowed us to obtain the solvent shifts components calculated according to eq 2, given in Table 6. The results for the two absorption energies are 4.35 and 5.11 eV. These values are halfway between the gas phase and the aqueous solution (4.30−4.39 eV and 5.06−5.15 eV) and already show a blue shift of ∼0.05 eV (δ_{geo}). Thus, an important part of the effect of water on the absorption spectrum of DMA can be ascribed to the influence on the molecular geometry: an increased wagging angle originates larger transition energies (a similar dependence was already described for the *p*-cyano derivative[37]). The other ∼0.05 eV of blue shift is then due to the difference in stabilization of the electron density in the ground and excited states ($\delta_{dist} + \delta_{elec}$).

In the S_1 structure, the geometry change in the solute is slightly smaller, but it also has an important effect on the transition energy. With the optimized geometry in solution, we obtain a gas-phase fluorescence energy of 3.72 eV, with a shift of −0.08 eV (δ_{geo}). In this case, however, the effect of the solvent on the electron density stabilization is much higher, accounting for an additional shift of −0.24 eV ($\delta_{dist} + \delta_{elec}$).

By examininig the distribution of water molecules around the solute, the effect of solvation on the transition energies

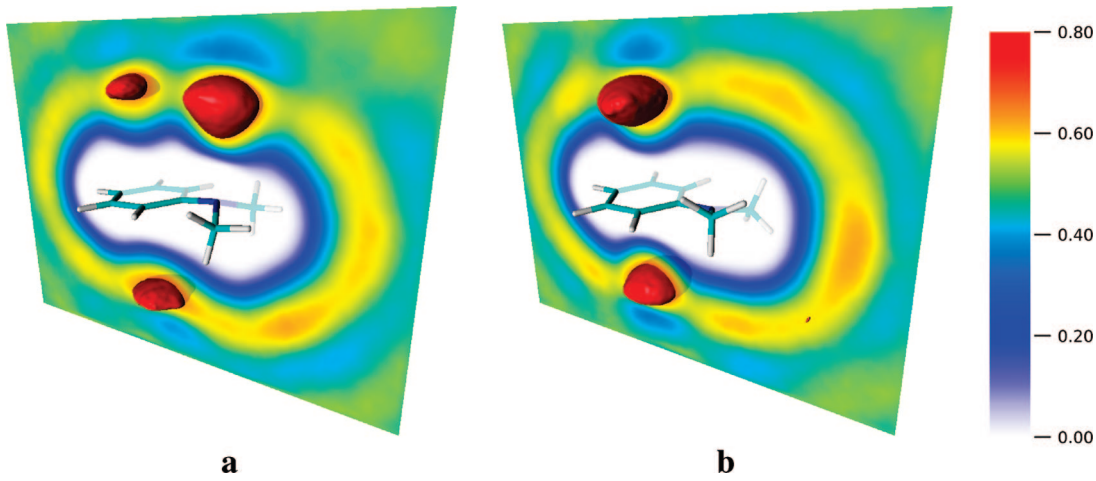

Figure 5. Occupancy maps of water oxygen atoms (considered as Van der Waals spheres, as calculated by VMD[38]) around DMA for (a) the optimized S_0 structure, and (b) the optimized S_1 structure. Solid isosurfaces shown for values of 0.64.

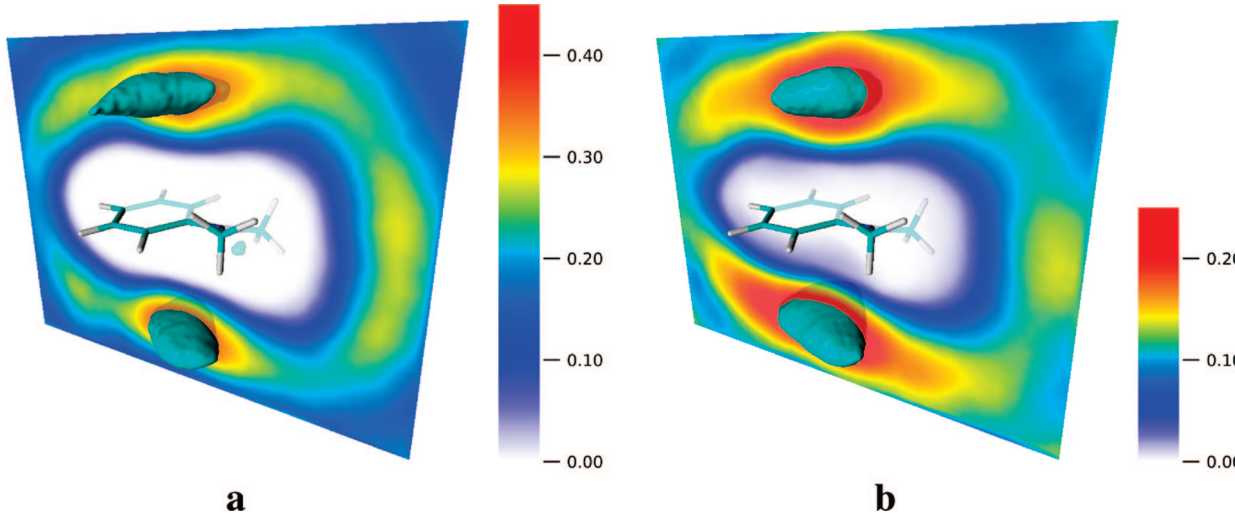

Figure 6. Occupancy maps of THF C_β atoms (considered as Van der Waals spheres, as calculated by VMD[38]) around DMA in the optimized S_1 state for (a) pure THF (isosurface value 0.35), and (b) THF/CH mixture (isosurface value 0.22). Note the different color scales in a and b.

Table 6. Solvent Shifts and Their Components, in eV, in Water, Calculated at CASPT2(0.00)/6-311G** Level

	δ	δ_{geo}	δ_{dist}	δ_{elec}
$S_0 \rightarrow S_1$	0.087	0.045	0.005	0.036
$S_0 \rightarrow S_2$	0.096	0.058	−0.020	0.057
$S_1 \rightarrow S_0$	−0.319	−0.075	−0.156	−0.087

can be further understood. Figure 5 shows in red the regions of space where oxygen atoms are more frequently found. There is a clear high concentration of water molecules near the N atom in the S_0 structure, indicating the existence of a hydrogen bond. This hydrogen bond stabilizes in particular the ground state, while the excited states, characterized by an electron density loss in the N, are less stabilized. Thus, the electrostatic contribution leads to a larger energy difference between the states, giving rise to a blue shift in the absorption bands, which is indicated by the positive sign of δ_{elec}. There are also regions of high oxygen concentration at both sides of the phenyl ring, solvating its partial negative charge (through the hydrogens, not shown). These solvent molecules contribute to stabilize in preference the excited states and somewhat counter the effect of the N atom solvation.

In the optimized S_1 structure, only the high oxygen concentration regions at both sides of the phenyl ring are found, and they are closer to the solute and stronger than in the S_0 structure. As before, these solvent molecules contribute to stabilizing the excited state more than the ground state. Moreover, the absence of water molecules solvating the N atom means that there is no counter stabilization of the ground state, and thus δ_{elec} is negative and larger in absolute value than for the absorptions.

3.3. Solvent Mixture. We also studied the behavior of DMA in a mixture of cyclohexane and tetrahydrofuran, with a molar fraction of 0.5. It is found experimentally that the solvatochromic shift, especially of the fluorescence band, is clearly nonlinear with the molar fraction, although the solvent mixture itself shows an almost ideal dielectric behavior,[1] where the polarity function $f(\varepsilon) = 2(\varepsilon - 1)/(2\varepsilon + 1)$ varies linearly with the molar fraction of the components.

The obtained results are included in Tables 3 and 4, all values are intermediate between those of cyclohexane and tetrahydrofuran, as expected. Regarding the transition energies, although the studied variations are rather small (0.02−0.06 eV), some nonlinearity can be observed in the fluorescence energies, where the maximum in the solvent mixture is closer to the value in THF than to that in CH. Both the direction and the amount of the nonlinearity are in agreement with experiment.[1]

This effect would be compatible with a preferential solvation of DMA by THF, meaning that the local concentration of this solvent around the solute should be higher than its bulk concentration. However, we find the opposite effect: the average number of tetrahydrofuran molecules within 3 Å of the solute is 5.1, while the number of cyclohexane molecules is 6.7 (a local THF molar fraction of 0.43). But, as it was shown for water (Figure 5b), solvation of the S_1 state occurs mainly at both sides of the phenyl ring. If we place one point at 3.5 Å at either side of the ring and consider only the solvent molecules within 1 Å of these points, we get in turn that the local THF molar fraction in these regions is 0.54. Thus, the preferential solvation by THF is observed in the regions most important for the stabilization of the excited-state of the solute, while in other regions THF is depleted. This is shown in Figure 6, taking into account that the partial density of THF in the solvent mixture is one-half of the pure solvent. The volumes inside the isosurfaces are similar, but the occupancy value for the mixture is 63%, more than one-half, of the value for pure THF. Likewise, the change in the color scale allows comparison of the occupancies in relation to the partial THF density.

Again, we compare with the results obtained with PCM, in Table 5. Somewhat surprisingly, the same nonlinearity in the $S_1 \rightarrow S_0$ transition is found in this case. The nonlinear behavior cannot be attributed here to the solvent response, since it is modeled as a linear-response continuum, so it must be due to the solute. In fact, the vacuum emission energy obtained with the PCM-optimized geometry in the solvent mixture is 0.02 eV lower than with the geometry in THF and 0.01 eV lower than in CH, and this can explain the nonlinearity in the final values. In any case, the energy variations are probably too small to draw definitive conclusions: a difference of only ∼0.01 eV separates linear and nonlinear behavior.

4. Conclusions

A theoretical study of the lowest-energy electron transitions in *N*,*N*-dimethylaniline has been performed. The first absorption transition has a very low intensity and implies mainly a local excitation on the phenyl ring, similarly to the fluorescence transition; the transition to the second excited state has a significant charge transfer component and consequently an enhanced intensity. Results in gas phase agree with experiments and support a pyramidal ground state and a twisted planar excited state for the DMA molecule.

In solution, a red shift of the absorption and fluorescence bands is found in polar nonprotic solvents, which is more important in the $S_0 \rightarrow S_2$ transition. The anomalous behavior experimentally found in water is well reproduced: a blue shift in the absorption bands seems to be due to the strong stabilization of the ground state through hydrogen bonds between water and the amine nitrogen, with an important contribution from the geometrical distortion of the solute; the strong red shift in the fluorescence band corresponds to an increased solvation of the phenyl ring in the excited state.

For the first time, calculations with a solvent mixture (cyclohexane and tetrahydrofuran) were performed with the ASEP/MD method. These calculations reproduce the nonlinearity found in the solvent shift with the mixture composition, and, although the magnitude of the effect does not allow to draw definitive conclusions, the results point to a local increase of the concentration of THF only in the regions perpendicular to the phenyl ring, where solvation of the excited state occurs, as a possible cause for the nonlinearity.

In summary, these results are in good agreement with experimental findings and show the ability of the ASEP/MD method to correctly describe the solute−solvent interactions involved in solvent shifts of absorption and emission bands. Moreover, the detailed representation of the system allows a more complete analysis of those interactions than with other models.

Acknowledgment. I.F.G. acknowledges the Junta de Extremadura and the European Social Fund for financial support. This work was supported by the CTQ2008-06224/BQU Project from the Ministerio de Ciencia e Innovación of Spain.

References

(1) Suppan, P. *J. Photochem. Photobiol. A* **1990**, *50*, 293–330.

(2) Sánchez, M. L.; Aguilar, M. A.; Olivares del Valle, F. J. *J. Comput. Chem.* **1997**, *18*, 313–322.

(3) Fdez. Galván, I.; Sánchez, M. L.; Martín, M. E.; Olivares del Valle, F. J.; Aguilar, M. A. *Comput. Phys. Commun.* **2003**, *155*, 244–259.

(4) Aguilar, M. A.; Sánchez, M. L.; Martín, M. E.; Fdez. Galván, I. An Effective Hamiltonian Method from Simulations: ASEP/MD. In *Continuum Solvation Models in Chemical Physics*, 1st ed.; Mennucci, B., Cammi, R., Eds., Wiley: New York, 2007; Chapter 4.5, pp 580−592.

(5) Fdez. Galván, I.; Sánchez, M. L.; Martín, M. E.; Olivares del Valle, F. J.; Aguilar, M. A. *J. Chem. Phys.* **2003**, *118*, 255–263.

(6) Muñoz Losa, A.; Fdez. Galván, I.; Martín, M. E.; Aguilar, M. A. *J. Phys. Chem. B* **2003**, *107*, 5043–5047.

(7) Fdez. Galván, I.; Olivares del Valle, F. J.; Martín, M. E.; Aguilar, M. A. *Theor. Chem. Acc.* **2004**, *111*, 196–203.

(8) Fdez. Galván, I.; Martín, M. E.; Aguilar, M. A. *J. Comput. Chem.* **2004**, *25*, 1227–1233.

(9) Fdez. Galván, I.; Aguilar, M. A.; Ruiz-López, M. F. *J. Phys. Chem. B* **2005**, *109*, 23024–23030.

(10) Martín, M. E.; Muñoz Losa, A.; Fdez. Galván, I.; Aguilar, M. A. *J. Mol. Chem. Struct. (THEOCHEM)* **2006**, *775*, 81–86.

(11) Martín, M. E.; Muñoz Losa, A.; Fdez Galván, I.; Aguilar, M. A. *J. Chem. Phys.* **2004**, *121*, 3710–3716.

(12) Muñoz Losa, A.; Fdez. Galván, I.; Martín, M. E.; Aguilar, M. A. *J. Phys. Chem. B* **2006**, *110*, 18064–18071.

(13) Muñoz Losa, A.; Fdez. Galván, I.; Aguilar, M. A.; Martín, M. E. *J. Phys. Chem. B* **2007**, *111*, 9864–9870.

(14) Muñoz Losa, A.; Fdez. Galván, I.; Martín, M. E.; Aguilar, M. A. *J. Phys. Chem. B* **2008**, *112*, 8815–8823.

(15) Roos, B. O.; Taylor, P. R.; Siegbahn, P. E. M. *Chem. Phys.* **1980**, *48*, 157–173.

(16) Andersson, K.; Malmqvist, P.-Å.; Roos, B. O.; Sadlej, A. J.; Wolinski, K. *J. Phys. Chem.* **1990**, *94*, 5483–5488.

(17) Andersson, K.; Malmqvist, P.-Å.; Roos, B. O. *J. Chem. Phys.* **1992**, *96*, 1218–1226.

(18) Ghigo, G.; Roos, B. O.; Malmqvist, P.-Å. *Chem. Phys. Lett.* **2004**, *396*, 142–149.

(19) Jorgensen, W. L.; Maxwell, D. S.; Tirado-Rives, J. *J. Am. Chem. Soc.* **1996**, *118*, 11225–11236.

(20) Breneman, C. M.; Wiberg, K. B. *J. Comput. Chem.* **1990**, *11*, 361–373.

(21) Lepori, L.; Matteoli, E. *Fluid Phase Equilib.* **1998**, *145*, 69–87.

(22) Frisch, M. J.; Trucks, G. W.; Schlegel, H. B.; Scuseria, G. E.; Robb, M. A.; Cheeseman, J. R.; Zakrzewski, V. G.; Montgomery, J. A., Jr.; Stratmann, R. E.; Burant, J. C.; Dapprich, S.; Millam, J. M.; Daniels, A. D.; Kudin, K. N.; Strain, M. C.; Farkas, Ö.; Tomasi, J.; Barone, V.; Cossi, M.; Cammi, R.; Mennucci, B.; Pomelli, C. S.; Adamo, C.; Clifford, S.; Ochterski, J. W.; Petersson, G. A.; Ayala, P. Y.; Cui, Q.; Morokuma, K.; Salvador, P.; Dannenberg, J. J.; Malick, D. K.; Rabuck, A. D.; Raghavachari, K.; Foresman, J. B.; Cioslowski, J.; Ortiz, J. V.; Baboul, A. G.; Stefanov, B. B.; Liu, G.; Liashenko, A.; Piskorz, P.; Komaromi, I.; Gomperts, R.; Martin, R. L.; Fox, D. J.; Keith, T. A.; Al-Laham, M. A.; Peng, C. Y.; Nanayakkara, A.; Challacombe, M.; Gill, P. M. W.; Johnson, B.; Chen, W.; Wong, M. W.; Andrés, J. L.; González, C.; Head-Gordon, M.; Replogle, E. S.; Pople, J. A. *Gaussian 98 (Revision A.11.3)*; Gaussian, Inc.: Pittsburgh, PA, 2001.

(23) Karlström, G.; Lindh, R.; Malmqvist, P.-Å.; Roos, B. O.; Ryde, U.; Veryazov, V.; Widmark, P.-O.; Cossi, M.; Schimmelpfennig, B.; Neogrády, P.; Seijo, L. *Comput. Mater. Sci.* **2003**, *28*222–239.

(24) Refson, K. *Comput. Phys. Commun.* **2000**, *126*, 310–329.

(25) Cervellati, R.; Borgo, A. D.; Lister, D. G. *J. Mol. Struct.* **1982**, *78*, 161–167.

(26) Kimura, K.; Tsubomura, H.; Nagakura, S. *Bull. Chem. Soc. Jpn.* **1964**, *37*, 1336–1346.

(27) Saigusa, H.; Miyakoshi, N.; Mukai, C.; Fukagawa, T.; Kohtani, S.; Nakagaki, R.; Gordon, R. *J. Chem. Phys.* **2003**, *119*, 5414–5422.

(28) Shanmugapriya, T.; Selvaraju, C.; Ramamurthy, P. *Spectrochim. Acta A* **2007**, *66*, 761–767.

(29) Kawski, A.; Kukliński, B.; Bojarski, P. *Z. Naturforsch.* **2003**, *58a*, 411–418.

(30) Ghoneim, N.; Suppan, P. *J. Chem. Soc., Faraday Trans.* **1990**, *86*, 2079–2081.

(31) Prabhumirashi, L. S.; Kutty, D. K. N.; Bhide, A. S. *Spectrochim. Acta A* **1983**, *39*, 663–668.

(32) Kawski, A.; Kukliński, B.; Bojarski, P. *Chem. Phys.* **2006**, *320*, 188–192.

(33) Tobita, S.; Kamiyama, R.; Takehira, K.; Yoshihara, T.; Yotoriyama, S.; Shizuk, H. *Anal. Sci.* **2001**, *17*, s50–s52.

(34) Oshima, J.; Shiobara, S.; Naoumi, H.; Kaneko, S.; Yoshihara, T.; Mishra, A. K.; Tobita, S. *J. Phys. Chem. A* **2006**, *110*, 4629–4637.

(35) Weidemaier, K.; Tavernier, H. L.; Fayer, M. D. *J. Phys. Chem. B* **1997**, *101*, 9352–9361.

(36) Linder, B. Reaction-Field Techniques and Their Applications to Intermolecular Forces. In *Intermolecular Forces*; Hirschfelder, J. O., Ed.; Advances in Chemical Physics 12; Interscience Publishers: New York, 1967; Chapter 5, pp 225−281.

(37) Miertus, S.; Scrocco, E.; Tomasi, J. *Chem. Phys.* **1981**, *55*, 117–129.

(38) Tomasi, J.; Mennucci, B.; Cammi, R. *Chem. Rev.* **2005**, *105*, 2999–3094.

(39) Serrano-Andrés, L.; Merchán, M.; Roos, B. O.; Lindh, R. *J. Am. Chem. Soc.* **1995**, *117*, 3189–3204.

(40) Humphrey, W.; Dalke, A.; Schulten, K. *J. Mol. Graph.* **1996**, *14*, 33–38.

CT800434J